



# Channel selection from source localization: A review of four EEG-based brain–computer interfaces paradigms

E. Guttmann-Flury<sup>1</sup> · X. Sheng<sup>1</sup> · X. Zhu<sup>1</sup>

Accepted: 27 May 2022  
© The Psychonomic Society, Inc. 2022

## Abstract

Channel selection is a critical part of the classification procedure for multichannel electroencephalogram (EEG)-based brain–computer interfaces (BCI). An optimized subset of electrodes reduces computational complexity and optimizes accuracy. Different tasks activate different sources in the brain and are characterized by distinctive channels. The goal of the current review is to define a subset of electrodes for each of four popular BCI paradigms: motor imagery, motor execution, steady-state visual evoked potentials and P300. Twenty-one studies have been reviewed to identify the most significant activations of cortical sources. The relevant EEG sensors are determined from the reported 3D Talairach coordinates. They are scored by their weighted mean Cohen’s *d* and its confidence interval, providing the magnitude of the corresponding effect size and its statistical significance. Our goal is to create a knowledge-based channel selection framework with a sufficient statistical power. The core channel selection (CCS) could be used as a reference by EEG researchers and would have the advantages of practicality and rapidity, allowing for an easy implementation of semiparametric algorithms.

## Highlights

- Cortical sources activations differ depending on the brain–computer interface (BCI) task and their modulations.
- The results from 21 studies are combined to define an optimized subset of EEG electrodes per BCI task.
- The magnitude and significance of the Cohen’s *d* effect size are calculated for each task-dependent EEG electrode.
- This knowledge-based channel selection framework could be used as a reference by EEG researchers.

**Keywords** Channel selection · EEG · BCI · Motor imagery · Motor execution · SSVEP · P300

## Introduction

Control of a computer or any other electronic device using only brainwaves is a long-hoped-for next-generation interaction tool (Leeb et al., 2006). Direct brain–computer interfaces (BCIs) can provide severely disabled people with new augmentative communication and control technology (Wolpaw et al., 2002). In the field of health care

and life sciences, a new nonmuscular channel could help restore voluntary motor control or improve the effectiveness of the rehabilitation process (Chaudhary et al., 2016). Beyond medical applications, recent experimental research has explored the usability of BCIs in the fields of multimedia and gaming (van Erp et al., 2012). Healthy customers could use this new input modality as part of an enhanced game experience (Bos et al., 2010).

The detection of cortical generators may help control external devices such as robots (Spataro et al., 2017), virtual environments (Leeb et al., 2006), or spelling devices (Kaplan et al., 2013) with various degrees of accuracy. Different strategies have been implemented to provide a convenient and straightforward way to command such devices. For instance, a user could steer a wheelchair by thinking about his or her right or left hand (Tsui et al., 2011). Functional connectivity changes within associated regions of the

✉ E. Guttmann-Flury  
eva.guttmann.flury@gmail.com

X. Zhu  
mexyzhu@sjtu.edu.cn

<sup>1</sup> State Key Laboratory of Mechanical System and Vibration,  
School of Mechanical Engineering, Shanghai Jiao Tong  
University, 800 Dongchuan Road, Minhang District,  
Shanghai 200240, People’s Republic of China

cortex would then allow the two classes to be distinguished (Pfurtscheller & Neuper, 2001). A motor imagery (MI) task is often preceded by the study of motor execution (ME). Sensorimotor rhythms are spontaneously generated in both tasks, and analyzing the latter should help establish a more profound understanding of the former. The specific mental states resulting from these tasks can be produced in an external stimulus-paced mode (synchronous BCI) or an internally paced mode (asynchronous BCI). The aforementioned brain signals are representative of endogenous BCI because they do not depend on any external stimuli (Torres et al., 2020).

Steady-state visual evoked potentials (SSVEP) (González-Mendoza et al., 2015) and P300 visual evoked potential (VEP) (Nicolas-Alonso & Gomez-Gil, 2012) represent the most commonly used exogenous BCIs. SSVEPs are elicited by the repetitive presentation of a visual stimulus that flickers or reverses at a fixed frequency. When a user focuses his or her gaze on a specific flickering image, an induced periodic brain electrical response is produced and can be associated with a unique command. Similarly, P300 is generated by a sequence of visual stimuli. When an infrequent event appears, it elicits an electrophysiological response that can be correlated with a specific choice. Other BCIs may use different types of brain activity, for instance emotion (Torres et al., 2020), speech (Wang et al., 2013) or hearing (Nijboer et al., 2008).

Many methods have been employed over the past seven decades to measure electrical or magnetic brain activity through invasive or noninvasive means (Waldert et al., 2009). Invasive approaches, such as electrocorticography (ECoG) (Schalk & Leuthardt, 2011), are believed to support more complex applications, because high spatial and temporal resolution may be achieved. However, because of several technical issues and the inherent risk of surgery, only a few severely disabled patients have been implanted with electrodes so far (Oxley et al., 2020). Noninvasive approaches, such as functional magnetic resonance imaging (fMRI) (Sitaram et al., 2007), positron emission tomography (PET) (Aine, 1995), magnetoencephalography (MEG) (da Silva, 2013) and electroencephalography (EEG) (Curran & Stokes, 2003), have all been extensively used as neuroimaging techniques (Vallabhaneni et al., 2005).

EEG represents the most prevalent method of signal acquisition for noninvasive BCI. Electrical brain oscillatory activity, generated by feedback loops in complex networks of neurons populations, is recorded by scalp electrodes (Vallabhaneni et al., 2005). The advantages of practicality, ease of use, high temporal resolution, and high coverage are counterbalanced by the limited topographical resolution and frequency range (Hill & Wolpaw, 2016). However, consistent activation patterns associated with specific cognitive tasks have been highlighted during fMRI or PET studies (Cabeza & Nyberg, 2000).

Assuming that the strength and accuracy of each modality would be preserved, the complementarity of information can be exploited by multimodal imaging techniques. The integrated knowledge gained from high spatial resolution measurements should help improve the accuracy of EEG-based BCI applications (Blinowska et al., 2009).

Current EEG-based BCIs are often recorded from multiple channels. A higher number of electrodes ensures a greater coverage of the brain and a more precise solution to the inverse problem. For uniformly distributed sensors over the full surface of the head, source localization accuracy has been shown to increase drastically from 31 to 63 sensors but much less from 63 to 123 electrodes (Michel, 2004). However, a greater number of channels can reduce the accuracy of the classification because while some sensors carry significant information, others introduce noise and thus deteriorate the results (Müller et al., 2000). This so-called curse of dimensionality can be alleviated by selecting an optimized subset of electrodes. The lower computational complexity also leads to easier real-time calculation and detection of predefined cognitive tasks.

Channel selection is used to identify this optimized subset of EEG electrodes. Most reviews and studies focus on the evaluation and efficiency of nonparametric algorithms to establish the optimal number of channels involved in a specific application (Alotaiby et al., 2015; Ghaemi et al., 2017; He et al., 2009; Barachant & Bonnet, 2011; Li et al., 2011; Arvaneh et al., 2010; Schröder et al., 2005; Qi et al., 2021; Gurve et al., 2020; Lal et al., 2004). To the best of our knowledge, no reviews have been carried out using prior findings from diverse recording modalities (fMRI, PET, EEG). For this purpose, the current paper uses a selection of past studies for four commonly used paradigms—MI, ME, SSVEP, and P300. For each task, the most recurring electrodes across studies are defined as the core channel selection (CCS) subset. The CCS represents the lowest common denominator, meaning that the CCS electrodes are supposed to be always activated and could be used either directly or through a specific combination to determine the paradigm characteristics.

## Method

One of the primary purposes of a meta-analysis is to draw conclusions from past studies often reporting disparate results. Pooling independent effect size estimates can inform about the direction and magnitude of an effect even more accurately than any of the individual estimates. Non-systematic biases that may arise, for instance from preprocessing steps, are assumed to become insignificant using this approach (Sacchet & Knutson, 2013).

## Literature search

The review is based on the PRISMA (preferred reporting items for systematic reviews and meta-analyses) statement and the recommendations of the Cochrane Collaboration (Liberati et al., 2009; Eccleston & Morley, 2009). Fully published articles were drawn from searches on Google Scholar in September 2020. English-language studies in which the subjects were asked to perform either motor imagery (MI), motor execution (ME), or to focus on SSVEP or P300, were included. This literature search yielded 117 articles.

All neuroimaging techniques were incorporated as long as the subjects were healthy human participants performing the correct task (e.g., only hand movement was considered for MI and ME; foot motion was rejected). Ninety-seven articles met these further requirements. The quality of the data was the most exclusive criteria. Studies that did not specify the exact location (3D coordinates from any atlas or EEG electrodes) of the brain structures involved in the task or did not provide enough data to compute the mean and standard error or deviation of these locations were excluded from further analysis (see Fig. 1). After applying these criteria, 21 articles remained. Figure 1a reproduces the standard PRISMA flow-chart diagram, while Fig. 1b highlights the precise number of papers excluded for each exclusion criterion.

The main purpose of this review is to create a knowledge-based channel selection framework with sufficient statistical power and practical significance. The latter can be established by quantifying the effect size. To compute all these measures, either the *Z*-score, the *t*-test, the Cohen's *r*, or Cohen's *q* should be available along with the corresponding standard error and deviation when necessary. The lack of reporting of such measures (or access to the original data) is a well-known issue in neuroscience (Poldrack et al., 2017) and might explain the generally small numbers of included studies in meta-analyses ( $(n=9)$  (Snyder & Hall, 2006),  $(n=30)$  (Mullin et al., 2016),  $(n=9)$  (Arns et al., 2013)).

The metadata for the 21 articles ( $n=21$ ) included in this meta-analysis is detailed in Table 1. In total, 311 healthy subjects participated in these studies, with a highly variable sample size ranging from 5 to 50 participants ( $mean = 14.8 \pm 11.1$ ). Most experiments used fMRI as a single recording technique (62%) or EEG (24%). The pre-processing details for cleaning, normalization and spatial filtering are mostly linked to the technical modality employed, and only three studies use channel re-referencing.

These studies compare brain activations according to three main themes: (a) task dissimilarities, (b) stimuli characteristics, and (c) individual differences. Among the first group, four studies (Gerardin et al., 2000; Stippich et al., 2002; Kraeutner et al., 2014; Burianová et al., 2013) compared MI to ME, while four others (Menon et al., 1997; Ramirez-Quintana et al., 2020; Ardekani et al., 2002; Mulert

et al., 2004) investigated the target vs. no target detection in P300, and two (Clark et al., 2000; Bledowski et al., 2004) the differences between target and distractor. One paper (Grafton et al., 1996) specifically investigated the difference between MI and viewing, whereas one (Begliomini et al., 2018) was dedicated to the differences between the left and the right hand in ME, and another one (Perlstein et al., 2003) to the dissimilarities between memory and control.

Fewer studies examined the impact of stimuli depending on their frequency (three articles (Srinivasan et al., 2007; Srinivasan et al., 2006; Martinez et al., 2007)), color (only one (Ikegami et al., 2012)), or location (also only one (Russo et al., 2007)). Differences between left- and right-handed individuals were examined in two papers (Willems et al., 2009; Begliomini et al., 2008), and a final one (Mokienko et al., 2013) was interested in the impact of BCI training on neural source activation.

## EEG channel determination

Multichannel EEG measures signals using either the 10-20, 10-10, or 10-5 international systems for standard electrode placement (Jurcak et al., 2007). The underlying neural generators are recorded as a mixture of signals emitted from several potential time-varying sources inside the brain (von Bünaü et al., 2010). The goal of the BCI paradigms is to produce distinct patterns of cortical activation to discriminate between various classes (Halder et al., 2011). For commonly used paradigms, knowledge of task-dependent cortical generators can inform the relevant recording positions for channel selection. In this paper, we review various studies that use source localization to identify significant cortical generators. The closest of the 62 selected EEG electrodes are then estimated for each of the results obtained from fMRI or PET. Our goal is to provide a knowledge-based channel selection framework that could be used either as a verification step or as part of the classification procedures.

The Koessler 3D anatomical atlas (Koessler et al., 2009) was used to correlate the 3D Talairach coordinates of the EEG electrode of the 10-10 system with their cortical projection points. For convenience, the Koessler 3D anatomical atlas is available as a CSV file at <https://github.com/QinXinlan/review-effect-size>. This 10-10 resolution combines the advantages of higher precision (yet still providing background compatibility to the 10-20) and reproducibility (by avoiding overlapping that may arise with the 10-5). The likely Brodmann area (BA) (respectively macro-anatomical structure) beneath each sensor is then calculated as the most frequently found in the population. Using the mean 3D Talairach coordinates and standard deviations of each sensor, it is possible to compute the Euclidian distance to each cortical generator reported in the reviewed articles. Standard deviations in *x*, *y*, and *z* play asymmetric roles, so the most

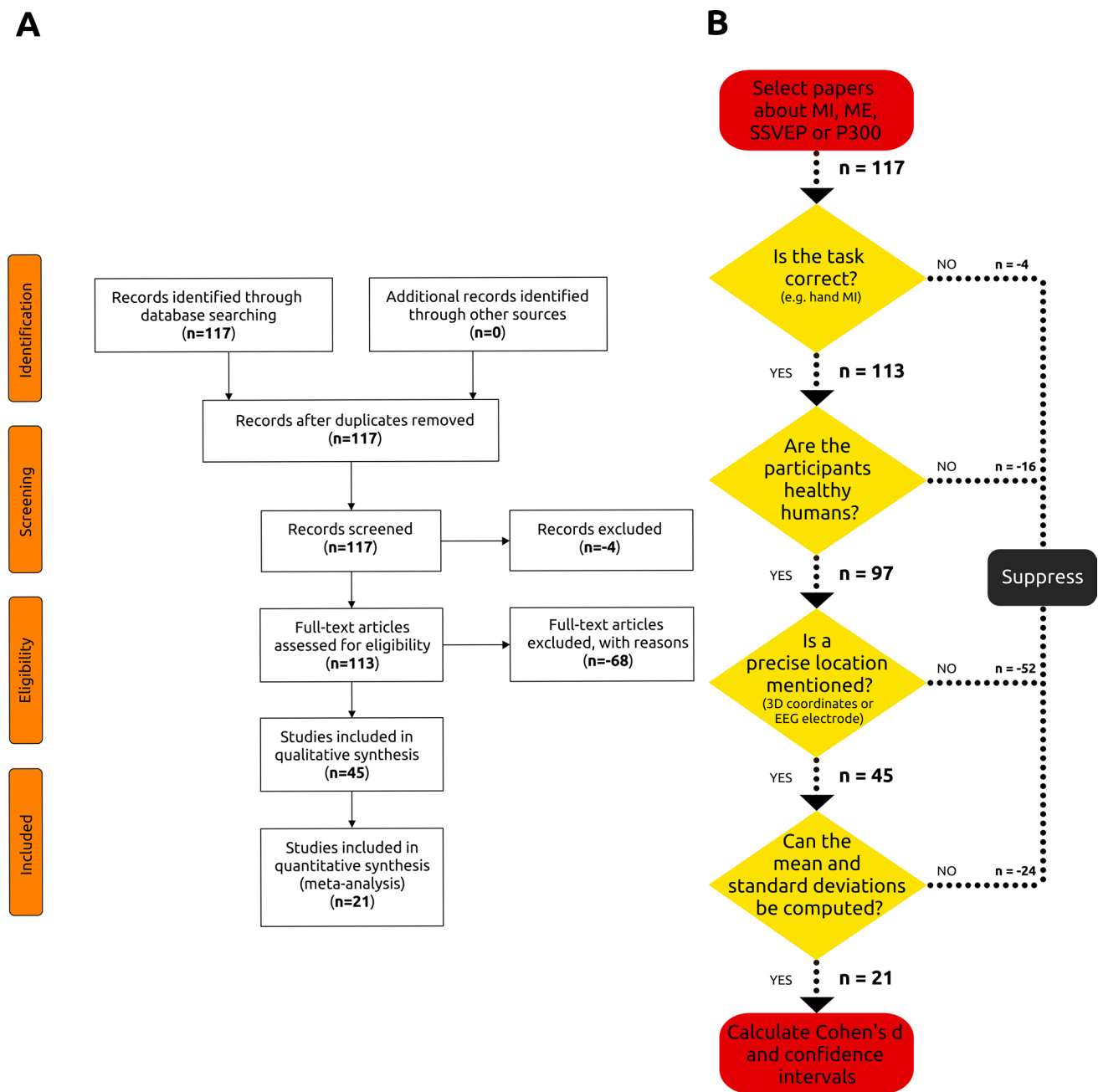


**Fig. 1** **a** Standard PRISMA flowchart diagram; **b** details of the exclusion criteria used with the associated number of studies, *n*.

likely electrode is not necessarily the closest one. When two EEG electrodes are nearly equidistant from a cortical source, both are recorded in the following tables with the electrode at the minimal Euclidian distance in the first position.

### Power analysis

Statistical power analysis reveals whether a finding actually reflects a true effect. By definition, the power of a statistical test is the probability that it will yield significant results. Its

complement  $\beta = 1 - \text{power}$  represents the error rate of failing to reject a false null hypothesis (type II). The statistical power is linked to three parameters: the significance criterion (type I error rate), the sample size, and the effect size. This last variable represents the degree to which the phenomenon can be detected. The larger the effect size is, the more easily the phenomenon can be exhibited (Cohen, 1977).

Every corresponding author of the 21 studies has been contacted and solicited to provide necessary information for computing the effect size. Most effects are reported as group

**Table 1** Main features of included studies; analyzed data are from \* (only for multiple recordings)

First author	Task	Recording method	Handedness	Sample size (N)	Year of publication	Paradigm	Cleaning	Normalization	Spatial filtering	Channel re-referencing
1. Gerardin (Gerardin et al., 2000)	MI & ME	MRI	Right	8	2000	Simple (simultaneous flexion/extension of the fingers) or complex (selective flexion/extension of the index and the little finger) continuous movement	Motion correction	Normalization to stereotaxic Talairach coordinates	Gaussian spatial filter to a final smoothness of 5 mm	No
2. Grafton (Grafton et al., 1996)	MI	PET	Right	7	1996	Precision grasp of common objects ranged in size from small to large	No	Spatial normalization using mean PET image from each individual + Global flow normalization	Smoothing to a final isotropic resolution of 18 mm	No
3. Stippich (Stippich et al., 2002)	MI & ME	fMRI	Right	14	2002	Right and left sided complex finger opposition involving digits 1–5	Correction of linear trends, high frequency fluctuations, and motion; exclusion when strong artifacts	Linear cross correlations between each image set and the supplied reference function	Threshold cluster size of 36 voxels	No
4. Mokienco (Mokienco et al., 2013)	MI	fMRI* & nTMS & EEG	Right	11	2013	Slow grasping movement with the right or left hand	Fat suppression and correction for motion	fMRI translation to standard Montreal Neurological Institute (MNI) coordinates	Smoothing	No
5. Willems (Willems et al., 2009)	MI	fMRI	Right & Left	32	2009	Imagining performance of manual and nonmanual action verbs	Realignment through rigid body registration	Normalization to Montreal Neurological Institute (MNI) space	Spatial smoothing (8 mm FWHM kernel)	No
6. Krautner (Krautner et al., 2014)	MI & ME	MEG* & EMG	Right	16	2014	Sequential button press with the nondominant (left) hand	Exclusion when head movements	Normalization to Talairach-Tournoux coordinate space	Dual-state beam-forming	No

**Table 1** (continued)

First author	Task	Recording method	Handedness	Sample size (N)	Year of publication	Paradigm	Cleaning	Normalization	Spatial filtering	Channel re-referencing
7. Burianová (Burianová et al., 2013)	MI & ME	fMRI & MEG	Right	14	2013	Specific finger movements	Realignment onto the mean image for head-motion correction	Spatial normalization into a standard stereotaxic space with voxel size of 2 mm <sup>3</sup> using the Montreal Neurological Institute (MNI) EPI template	Spatial smoothing filter for each volume by convolving it with an isotropic Gaussian kernel	No
8. Begliomini (Begliomini et al., 2008)	ME	fMRI	Right & Left	34	2008	Grasping with the index and the thumb of spherical plastic objects (3 cm diameter)	Motion correction	Normalization using the MNI152 template	Single-subject spatial normalization using the high-resolution T1 template	No
9. Begliomini (Begliomini et al., 2018)	ME	fMRI	Left	16	2018	Grasping with the index and the thumb of a spherical object (3 cm diameter)	Correction for head motion (translations/rotations)	Normalization using the MNI152 template	Smoothing using a 3D Gaussian kernel	No
10. Di Russo (Russo et al., 2007)	SSVEP	fMRI & EEG	Right	15	2007	Circular Gabor grating sinusoidally modulated in black and white	(1) fMRI = Removal of constant and linear terms + motion correction through a rigid body transformation with a least-squares approach (2) EEG = Rejection of epochs with artifacts (eye movements, blinks, or amplifier blocking + Bandpass filter from 5 to 25 Hz on time-averaged VEPs	(1) fMRI = Normalization according to the overall sensitivity of each subject (2) EEG = Normalization to the standardized finite element model of BESA 2000	No	No



**Table 1** (continued)

First author	Task	Recording method	Handedness	Sample size (N)	Year of publication	Paradigm	Cleaning	Normalization	Spatial filtering	Channel re-referencing
11. Srinivasan (Srinivasan et al., 2007)	SSVEP	fMRI	NA	6	2007	High-contrast sinusoidally reversing checkerboard with stimulus frequencies ranging from 3 to 14 Hz	No	Normalization to the MNI template	Smoothing using a Gaussian filter of size 7.65 mm FWHM	No
12. Srinivasan (Srinivasan et al., 2006)	SSVEP	EEG	Right	11	2006	Patterns composed of 600 dots with stimulus frequencies ranging from 3 to 30 Hz	Removal of 10 EEG channels due to artifacts in some subjects	Signal-to-noise ratio units	Surface Laplacian calculated with the New Orleans 3D Spline Laplacian algorithm	Average reference of the 110 recorded EEG channels
13. Perlstein (Perlstein et al., 2003)	SSVEP	EEG	Right	18	2003	Grayscale pictures representing pleasant, neutral, and unpleasant images flickering at 10 Hz	Offline correction for electro-oculographic contamination	Linear regression-based de-meaning and de-trending of the averaged data	LORETA source localization with a 7 mm spatial resolution	Average reference of the 128 recorded EEG channels
14. Martinez (Martinez et al., 2007)	SSVEP	EEG	NA	5	2007	Navigation of a small car on the computer screen in real time using an array of four small checkerboard images flickering with different frequencies	Blind source separation (BSS) algorithm for artifact rejection	Energy normalization of each flickering frequency directly by using a dedicated tuned filter	No	No
15. Menon (Menon et al., 1997)	P300	fMRI* & EEG	Right	11	1997	Auditory oddball paradigm with eighty 1000 Hz (frequent) and twenty 2000 Hz (infrequent) tones	Movement correction using least square minimization	Normalization to stereotaxic Talairach coordinates	Spatial smoothing with a uniform 3D Gaussian filter	No

Table 1 (continued)

First author	Task	Recording method	Handedness	Sample size (N)	Year of publication	Paradigm	Cleaning	Normalization	Spatial filtering	Channel re-referencing
16. Ikegami (Ikegami et al., 2012)	P300	EEG & fMRI*	Right	12	2012	Visual-flicker stimuli in a 6 × 6 alphabet flicker matrix modified from the “P300 speller” with two types conditions (green/blue luminance and chromatic and white/gray luminance)	Removal of low-frequency noise with a high-pass filter (cutoff period of 128 s) + correction of short-range serial correlations with an autoregressive (order one) model	Normalization to a Montreal Neurological Institute (MNI) EPI template	Smoothing with an 8-mm full width at half maximum (FWHM) Gaussian kernel	No
17. Ramirez-Quintana (Ramirez-Quintana et al., 2020)	P300	EEG	NA	8	2020	Donchin Speller configured in columns (letter speller)	Third-order Butterworth band-pass filter from 1 to 15 Hz	Normalization to obtain a zero mean and unitary variance in all the channels	No	No
18. Ardekani (Ardekani et al., 2002)	P300	fMRI	NA	7	2002	Classic visual oddball paradigm with a standard visual stimulus of characters ‘OOOOO’ and a target image with characters ‘XXXXX’	Motion correction + centering of the voxels’ time-series to obtain a zero mean + trend removal by PCA	Normalization to the Talairach–Tourneaux coordinates	Resampling to a voxel size of 3x3x3 mm <sup>3</sup> and a matrix size of 54x64x50	No
19. Clark (Clark et al., 2000)	P300	fMRI	Right	6	2000	Classic visual oddball paradigm with a standard visual stimulus using the letter ‘T’, a distractor letter ‘C’, and a target letter ‘X’	Movement correction	Normalization to the Talairach–Tourneaux coordinates	Threshold clusters of 10 or more contiguous voxels	No
20. Mulert (Mulert et al., 2004)	P300	EEG	NA	50	2004	Auditory oddball paradigm with 80% nontarget stimuli (500 Hz) and 20% target stimuli (1000 Hz)	Rejection of trials using an amplitude criterion ( $\pm 70 \mu V$ ) for every EEG and EOG channel	Two approaches: Averaging of the LORETA-images and grand averaging of the event-related potentials (ERPs)	LORETA source localization with a 7 mm spatial resolution	Average reference of the 63 recorded EEG channels



Table 1 (continued)

First author	Task	Recording method	Handedness	Sample size (N)	Year of publication	Paradigm	Cleaning	Normalization	Spatial filtering	Channel re-referencing
21. Bledowski (Bledowski et al., 2004)	P300	fMRI* & EEG	Right	10	2004	Three-stimulus oddball task with simple blue shapes	3D motion correction to estimate the three translation and three rotation parameters of rigid body transformation	Normalization to the standard Montreal Neurological Institute (MNI) template head surface	Spatial smoothing of EPI images with a Gaussian kernel (8 mm FWHM kernel)	No

differences; thus, Cohen's  $d$  has been favored in this review (Cohen, 1977). Heuristically, this number measures the statistical level of distinction between two variables. Given two sample groups, the greater the distance between their means, the more easily they can be separated. The Cohen's  $d$  index measures this distance in terms of standard deviations units and is considered dimensionless: Cohen's  $d = \frac{M_1 - M_2}{SD}$  (where  $M_1$  is the mean of group 1,  $M_2$  the mean of group 2, and SD, the standard deviations, are assumed equal in this equation, as they are similar in reality). A more-specific Cohen's  $d$  formula can be used, or other metrics can allow the characterization of the phenomenon. For instance, in a P300 experiment, group 1 could be defined as the target stimuli and group 2 as the nontarget stimuli.

For all studies, the mean across subjects (computed from Z-score,  $t$ -test, percentage of signal change, or raw data) was calculated on every selected electrode. For each task and each electrode, the mean effect size was computed, and weighted by the number of subjects in individual studies. To assess the statistical significance of the results, a 95% confidence interval was also outlined. In this review, most of the confidence intervals exclude 0, meaning that the mean effect size is statistically significant at  $\alpha = 0.05$  (Ellis, 2010). If the mean effect size, the lower bound of the confidence interval, and the weights used in the corresponding computation are large enough, the selected EEG channel will be validated. The R code used to calculate the effect sizes per study (Ben-Shachar et al., 2020) and the weighted mean effect size is available online at <https://github.com/QinXinlan/review-effect-size>.

### Sample size estimation

How many studies would be necessary to obtain a sufficient statistical power? Conventionally, in meta-analysis methods, fixed effects and random effects models are used. In the former case, the included studies are assumed to represent the entire universe of studies of interest and hence, there is no possibility of sampling error (Hunter & Schmidt, 2000). In view of the high variability of the phenomena under study, the included studies are considered to only represent a small portion of all the available data and thus, the slightly more sophisticated random effects model is preferred.

To evaluate the sample size, i.e., the number of studies, choices and hypotheses must be made on some parameters. Typically, the type I error rate is set at  $\alpha = 0.05$  and the relative seriousness of type I to type II error is 4 to 1 ( $\beta = 0.2$  and thus  $power = 0.8$ ). The standard normal cumulative distribution function for  $\beta = 0.2$  yields a value of  $-0.842$ , and a mean of the Z statistic of  $1.64 - (-0.842) = 2.482$  for a one-tailed test.

Under the random effects hypothesis, the  $Z$  statistic has a normal distribution with a mean equal to  $\lambda^* = \frac{\bar{d}-0}{\sqrt{v^*/k}}$ , where  $k$  is the number of studies (random effects estimates are usually noted with an asterisk (Hedges & Pigott, 2001)). The “typical” sampling variance of the random effects estimate is calculated (Valentine et al., 2010) with  $v^* = v + \tau^2 = \frac{2}{n} + \frac{\bar{d}^2}{4} * n + \tau^2$ . Given a random effects analysis, the number of studies should then be  $k = \frac{v^*}{(\bar{d}/\lambda^*)^2}$ , where  $\lambda^* = 2.482$ .

A scoping review on different electrodes led us to believe that the estimated population effect size may vary from  $\bar{d} = 1.5$  to  $\bar{d} = 3$  with a variance  $\tau^2 = 1$  and for an average number of subjects per study  $n = 15$ . For an estimated population effect size of  $\bar{d} = 1.5$ , approximately four studies ( $k = 3.2$ ) are needed under the random effects assumptions to obtain an approximate power of 0.80. For a greater estimated effect size of  $\bar{d} = 3$ , only one study ( $k = 0.88$ ) is needed to obtain a sufficient power, with all other hypotheses remaining equal.

## Hypothesis

This review and its potential applications rely on three assumptions: (1) despite the substantial inherent variability in the exact source localization of neural generators, the sensorimotor and visual networks are postulated to be consistent across subjects and sessions, and the other cortical networks relevant to our BCI paradigms should probably be considered more subject-dependent; (2) the estimated EEG electrodes or their nearest neighbors are likely to reflect most of the relevant cortical information; (3) the classification accuracy is presumed to be optimized by the choice of an adequate subset of electrodes.

## Results

### Motor imagery (MI)

MI-based BCI is a popular interaction paradigm because it relies on voluntary movement and can be used, in theory, by healthy and impaired subjects alike in synchronous or asynchronous paradigms. In particular, the movement of the right and left hands is often selected because of its easily distinguishable activity in the contralateral cortical regions responsible for the movement of the limbs. MI is usually defined as the mental rehearsal of a motor act (Crammond, 1997). This cognitive process appears to correspond to the activation of the neural correlates of motor representations (Rizzolatti & Craighero, 2004). It includes the planning and preparation of movements but not the motor output or

somatosensory feedback. The neural network involved during MI activates several cortical areas depending on the task and on the participant’s handedness and familiarity with BCI and the task. Several studies (Gerardin et al., 2000; Stippich et al., 2002; Kraeutner et al., 2014; Burianová et al., 2013; Grafton et al., 1996; Willems et al., 2009; Mokienko et al., 2013) have described the mapping of cerebral networks by localizing the main sources in each functional area across participants. Table 2 compiles these results with similar inclusion criteria (i.e., for healthy subjects).

The estimated EEG electrodes are then classified into three main clusters as shown in Fig. 2. The first one gathers all electrodes that are not contralateral (i.e., either bilateral or unilateral). The second cluster represents all contralateral sources that depend on the user experience (familiarity with BCI). The third one corresponds to all contralateral sources consistently present among subjects. Ipsilateral clusters can also be activated alongside contralateral sources to a lesser extent (Porro et al., 2000). If an electrode may be classified as both contralateral and unilateral, the bilaterality may be more influential and the electrode is labelled as such. Finally, the effects of handedness for the dominant hand on electrode activation is emphasized with an upper black point. For instance, FC2 is mostly activated for left-handed participants when moving their left dominant hand.

For the MI task, the CCS subset consists of electrodes {FC4, FC2, FC1, C4, C6, C5, C3, CP3, CP1}.

### Motor execution (ME)

A voluntary movement is comprised of three phases: planning, execution, and recovery. During the first phase, similar functional circuits, located in the frontoparietal, subcortical, and cerebellar areas, are activated in both ME and MI, suggesting they share a common pattern in the planning and preparation tasks. However, MI also activates distinct regions that can be predominantly found in the left hemisphere, namely the middle temporal gyrus and the fusiform gyrus (BA 21 and 37, electrodes TP7, P7, and T7). The predicted visual consequences of an action are believed to be represented in the former gyrus (Schippers & Keysers, 2011), whereas lesions in the latter impair pantomime recognition (Varney & Damasio, 1987). Thus, these regions could be hypothesized to participate in the planning of an imaginary movement. Furthermore, lesions in the superior and inferior parietal cortex (BA 7 and 40; electrodes CP4, P1, and P2) lead to impairment in the ability to imagine movements. Therefore, these cortices could be responsible for ensuring that the action being executed matches the intended action (Danckert et al., 2002).

During ME, the secondary sensory area (S2, BA 43; electrode CP6) seems to display heightened activation and is assumed to be related to the processing of proprioceptive

**Table 2** 3D Talairach coordinates of significant cluster maxima for motor imagery of left and right hand movements with corresponding international 10-10 EEG system closest electrode(s); BA: Brodmann area; Hem: hemisphere; L: left; R: right; NP: not pertinent; \* for BCI-trained subjects, \*\* for BCI-native subjects; ++ specific to MI; left underline for left-handed subject's dominant hand; right underline for right-handed subject's dominant hand; and Cohen's *d* mean effect size with a 95% confidence interval and the number of relevant studies in superscript

Lobe	Anatomic area	Area	Macro-anatomical structure	Laterality	BA	Hem	Talairach			Closest electrode(s)	Cohen's <i>d</i> weighted effect size
							X	Y	Z		
Frontal	Prefrontal cortex	Rostral prefrontal	Superior frontal gyrus	Unilateral	10, 11	R	30	51	24	FP2	3.24 [1.85; 4.62] <sup>1</sup>
		Dorsolateral prefrontal **	Middle frontal gyrus	Contralateral	6	L	-20	18	59	FL	1.25 [0.34; 2.15] <sup>2</sup>
	Inferior frontal		Bilateral	9, 8, 46	L	-54	42	15	F5, F3	2.79 [1.28; 4.28] <sup>2</sup>	
				44, 45	R	48	24	6	F8	3.36 [1.97; 4.74] <sup>1</sup>	
	Premotor and motor cortex	Lateral premotor	Middle frontal gyrus	L	-54	12	12	F7	3.05 [1.66; 4.43] <sup>1</sup>		
				R	42	6	57	EC4, EC2	1.28 [0.6; 1.95] <sup>5</sup>		
	Medial premotor	Pre-SMA	Superior frontal gyrus	L	-42	3	51	FC3	3.31 [1.82; 4.76] <sup>2</sup>		
				R	3	6	69	FCZ	4.8 [2.91; 6.66] <sup>2</sup>		
	Post-SMA		Bilateral	6	L	-3	6	69	FCZ	4.8 [2.91; 6.66] <sup>2</sup>	
				6	R	20	-7	44	EC2	1.57 [0.68; 2.45] <sup>2</sup>	
Parietal	Primary motor (M1) *	Precentral gyrus	6	L	-6	-3	69	FCL	1.37 [0.68; 2.06] <sup>5</sup>		
			4	R	18	-22	54	C2	1.66 [0.69; 3.07] <sup>2</sup>		
	Primary sensory (S1)	Postcentral gyrus	4	L	-19	-15	-58	C1	3.39 [1.61; 5.11] <sup>1</sup>		
			1, 2, 3	R	54	-21	39	C4, C6	1.26 [0.36; 2.28] <sup>4</sup>		
	Superior parietal ++	Precuneus	Bilateral	7	R	24	-54	51	P2, CP2	2.29 [1.28; 3.48] <sup>3</sup>	
			L	-60	-21	39	C5, C3	2.55 [1.16; 3.93] <sup>1</sup>			
	Inferior parietal ** ++	Inferior parietal gyrus	Bilateral	7	L	-27	-60	54	P1	3.03 [1.54; 4.49] <sup>2</sup>	
			R	36	-30	42	CP4	1.47 [0.58; 2.35] <sup>2</sup>			
	Middle temporal		Middle temporal gyrus	40	L	-36	-42	48	CP2, CP1	1.38 [0.37; 2.39] <sup>4</sup>	
				21	L	-60	-57	6	TP7, T7	3.29 [1.9; 4.67] <sup>1</sup>	
Occipital	Inferior temporal	Inferior temporal gyrus	19	R	56	-60	5	P8	1.55 [0.73; 2.36] <sup>1</sup>		
			19, 37	L	-55	-65	6	PZ	0.73 [-0.01; 1.46] <sup>1</sup>		
	Superior occipital	Occipitoparietal sulcus	Unilateral	19	L	-25	-61	33	PO3	2.61 [1.05; 4.11] <sup>1</sup>	
			Bilateral	17, 18	R	12	-84	6	O2	2.01 [0.7; 3.33] <sup>1</sup>	
		Calcarine gyrus	L	-12	-88	-2	O1	2.54 [1.08; 3.99] <sup>1</sup>			

Table 2 (continued)

Lobe	Anatomic area	Area	Macro-anatomical structure	Laterality	BA	Hem	Talairach			Closest electrode(s)	Cohen's <i>d</i> weighted effect size
							X	Y	Z		
Subcortical regions	Caudate nucleus			Bilateral		R	15	9	15	NP	
						L	-18	9	21	NP	
	Basal ganglia	Putamen	Anterior	Bilateral		R	27	9	12	NP	
						L	-27	6	12	NP	
Cerebellum	Insula **			Bilateral	13						
	Thalamus	Ventral lateral nucleus		Contralateral							
				Ipsilateral							

input (Dresel et al., 2005). More specifically, action planning has been associated with an increase of activity in the left-lateralized supramarginal gyrus (Króliczak et al., 2016) (BA 40; electrode CP5). A possible explanation of these differences between MI and ME relies on the evolutionary theory of motor task learning. Mentally rehearsing the action would allow for multiple attempts without the risk of causing any harm and, hence, would help find the best strategy for a difficult motor task (Gerardin et al., 2000). Some studies (Gerardin et al., 2000; Stippich et al., 2002; Kraeutner et al., 2014; Burianová et al., 2013) compared the somatotopic mapping during MI and ME, while others (Begliomini et al., 2008, 2018) examined the effects of handedness. Their results are summarized in Table 3.

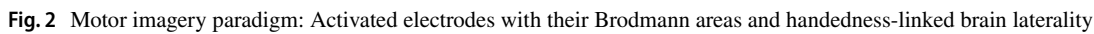
For the ME task, only two clusters have been identified, as illustrated in Fig. 3—either non-contralateral (bilateral or unilateral) or contralateral. The ME topographical distribution, as expected, largely overlaps the MI one. However, the assumption that MI is a more complex cognitive task might explain why the number of cortical generators activated with ME is much smaller for a simple task (Hardwick et al., 2017). Interestingly, mental chronometry studies have shown that the time course of MI positively correlates with ME, illustrating the parallelism between these two tasks (Vargas et al., 2004).

For right-handed subjects (an estimated 90% of the worldwide population), right hand MI and ME activates a restricted cluster compared to left hand MI and ME (Burianová et al., 2013). Right-handed subjects also show a predominant activation of motor and visuomotor control in the contralateral (i.e., left) hemisphere, while left-handed subjects have been characterized by a more bi-hemispheric recruitment of neuronal circuits when performing a precision grasping task. This might indicate a left hemispheric location of visuomotor control (Begliomini et al., 2018). In general, the more repetitive the task is, the more specialized and smaller the neural circuit would be. Therefore, the nondominant hand, being used less often, would require the additional control provided by a more widespread neural activation. Finally, it should be noted that the complexity of the task, implying other functions, influences the lateralization and the level of activation in some regions is age-dependent (Ward & Frackowiak, 2003).

For the ME task, the CCS subset consists of electrodes {FC4, FC2, FC1, FC3, C2, C1, C4, C3}. A common CCS for all motor-related tasks (MI and ME) could also be defined with the electrodes {FC1, FC2, FC4, C3, C4}.

### Steady-state visual evoked potentials (SSVEP)

Changes in the visual field are known to impact EEG activity. In particular, the periodic contrast or luminance modulation of a fixed frequency (usually at a range of 6–40 Hz) elicits an SSVEP that can be detected at the same fundamental



SSVEP-based BCIs often have a high temporal and spectral resolution (usually less than 0.1 Hz) as well as high accuracy and a high information transfer rate (ITR) (Nunez et al., 2006), but can produce visual fatigue or discomfort (Zhu et al., 2010). The temporal frequency, spatial frequency, contrast, luminance, color, and hue of the driving flickering stimulus all influence the amplitude and phase of the SSVEP (Zhu et al., 2010; Regan, 1989). This dependency on the input frequency partly reflects the delay between the retina and primary visual cortex as well as the delays between areas of the visual system (Schmolesky et al., 1998). Moreover, the area of on-screen stimulus also has an impact on the cortical modulation. For instance, a 6 Hz

For the SSVEP task, the CCS subset consists of electrodes {P1, PZ, P2, PO3, POZ, PO4, O1, OZ, O2}.

Attention to a change in the environment elicits a burst of activity, peaking at about 300 ms after the sensory stimulus. This P300 event-related potential (ERP) is an umbrella term encompassing two separate attentional processes. The P3a, or Novelty P3, occurs in response to all rare sounds or images—designated as deviant stimuli—regardless of whether they are targets (Spencer et al., 2001; Gaeta et al., 2003). The P3b appears after the appearance of a low-probability target item embedded in a train of high-probability nontarget (or standard) items. Both the amplitudes of the P3a and P3b, as well as their peak latencies, can be characterized as functions increasing (respectively decreasing) with age

**Table 3** 3D Talairach coordinates of significant cluster maxima for motor execution of left and right hand movement; ++ specific to ME; NP: not pertinent; BA: Brodmann area; Cohen's *d* mean effect size with a 95% confidence interval and the number of relevant studies in superscript

Lobe	Anatomic area	Area	Macro-anatomical structure	Laterality	BA	Hem	Talairach			Closest electrode(s)	Cohen's <i>d</i> weighted effect size	
							X	Y	Z			
Frontal	Prefrontal cortex	Inferior frontal	Inferior frontal gyrus	Unilateral	44, 45	R	57	18	24	F8	3.05 [1.93; 4.15] <sup>2</sup>	
						L	-49	5	16	EC5	2.47 [1.51; 3.41] <sup>1</sup>	
	Premotor and motor cortex	Lateral premotor	Superior frontal gyrus	Contralateral	6	R	42	-3	60	FC4, FC2	2.44 [1.84; 3.03] <sup>4</sup>	
						L	-36	-3	66	FC1, FC3	2.52 [1.77; 3.27] <sup>3</sup>	
	Pre-SMA	Medial premotor	Bilateral	6	R	6	6	6	57	FCZ	3.7 [2.32; 5.09] <sup>1</sup>	
					L	-9	9	51	FCZ	3.7 [2.32; 5.0] <sup>1</sup>		
Parietal	Post-SMA	Bilateral	6	R	3	-3	66	FCZ	3.7 [2.32; 5.09] <sup>1</sup>			
				L	-3	-3	66	FCZ	3.7 [2.32; 5.09] <sup>1</sup>			
				R	39	-15	63	C2	1.64 [1.2; 2.27] <sup>5</sup>			
	Primary motor (M1)	Precentral gyrus	Contralateral	4	L	-42	-18	66	C1	1.75 [1.29; 2.54] <sup>6</sup>		
					R	42	-33	60	C4	1.6 [1.15; 2.26] <sup>4</sup>		
					L	-48	-24	57	C3	1.62 [1.16; 2.42] <sup>5</sup>		
Subcortical regions	Parietal cortex	Primary sensory (S1)	Postcentral gyrus	Bilateral	7, 4	R	4	-40	38	CPZ, CZ	0.78 [0.59; 0.97] <sup>1</sup>	
						R	36	-36	66	CP2	1.15 [0.59; 1.72] <sup>1</sup>	
						L	-30	-42	66	CP1	1.06 [0.49; 1.62] <sup>1</sup>	
	Anterior part	Inferior parietal	Anterior intraparietal sulcus (AIP)	Bilateral	40	R	42	-45	48	CP4	0.9 [0.62; 1.18] <sup>1</sup>	
						L	-45	-36	60	CP3	1.12 [0.72; 1.53] <sup>2</sup>	
						R	60	-9	15	CP6	1.14 [0.57; 1.71] <sup>1</sup>	
Cerebellum	Basal ganglia	Secondary sensory (S2) ++	Parietal operculum	Bilateral	40, 43	L	-60	-15	21	CP5	1.13 [0.57; 1.7] <sup>1</sup>	
						R	24	18	6	NP		
						L	-30	6	6	NP		
	Thalamus	Putamen	Posterior part ++	Bilateral			R	27	-9	12	NP	
							L	-33	-3	6	NP	
							R	15	-12	9	NP	
Rostral part	Bilateral					L	-18	-15	9	NP		
						R	21	-45	-18	NP		
						L	-27	-45	-18	NP		

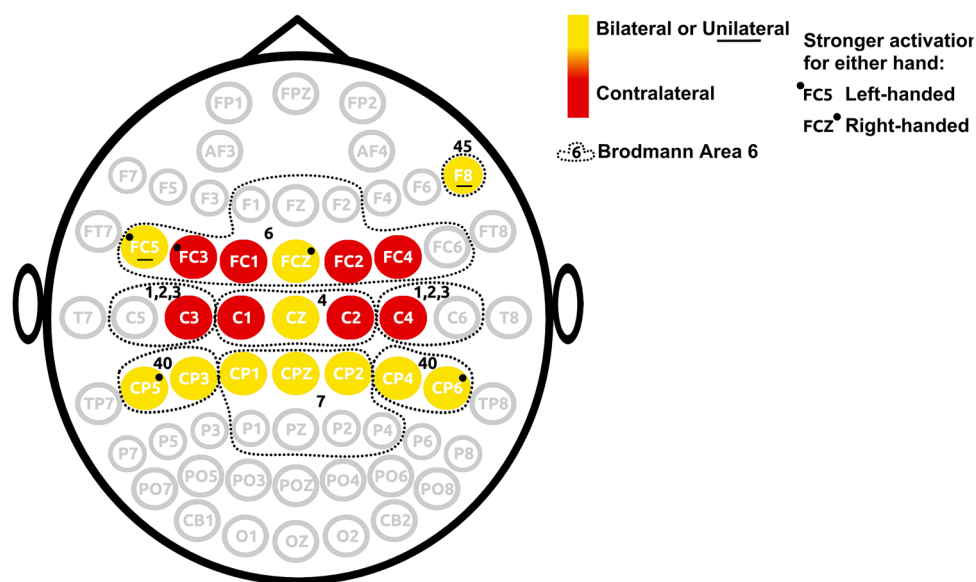


**Fig. 3** Motor execution paradigm: activated electrodes with their Brodmann areas and handedness-linked brain laterality

**Table 4** Mainly activated EEG electrodes according to the stimulus frequency

10 Hz	11 Hz	12 Hz	13 Hz
CZ	P1	F1	F6
CPZ	PZ	FZ	F8
P1	P2	P3	FC6
PZ	PO3	P1	FT8
P2	POZ	PZ	P3
PO3	PO4	P2	P1
POZ	O1	P4	PZ
PO4	O2	PO3	P2
CB1		POZ	PO5
O1		PO4	PO3
OZ		PO5	POZ
O2		PO6	PO4
		CB1	PO6
		O1	PO8
		OZ	CB1
		O2	O1
			OZ
			O2
			CB2

(Fjell & Walhovd, 2004). Additionally, the topographical distribution of the two P3 components seems to also be age dependent (West et al., 2010).

Typically elicited between 250 ms and 500 ms, the P3b is believed to reflect the process of directed attention leading to conscious awareness of salient stimuli (Menon et al., 1997). Detecting this cognitive component can reflect user intention

and provide useful biomarkers for normal aging or several brain or mental diseases (Friedman, 2003; Rossini et al., 2007). Table 6 summarizes the locations and time-courses (when available) of its neural generators from seven studies (Menon et al., 1997; Ramirez-Quintana et al., 2020; Ardekani et al., 2002; Mulert et al., 2004; Clark et al., 2000; Bledowski et al., 2004; Ikegami et al., 2012). Furthermore, the source contributions calculated from the functional magnetic resonance imaging (fMRI) activation clusters are also indicated. However, as the authors warn, the intrinsic technical and theoretical differences between ERP and fMRI might cause some discrepancies. For instance, the temporally dispersed activity reflected by fMRI (which is typically integrated over 1 second and then averaged) might get lost when compared to ERP (which is only averaged) (Bledowski et al., 2004).

Two different types of information are depicted in Fig. 5. One highlights the contribution to the generation of the P300 for each electrode (low or high), while the other indicates the time-dependent activation for several EEG electrodes, using five 50-ms time intervals (Mulert et al., 2004). The chrono stimulation is illustrated on two consecutive images for the sake of simplicity.

For the P300 task, the CCS subset consists of electrodes {CP3, CP4, P1, P3, P2, P4, P6}.

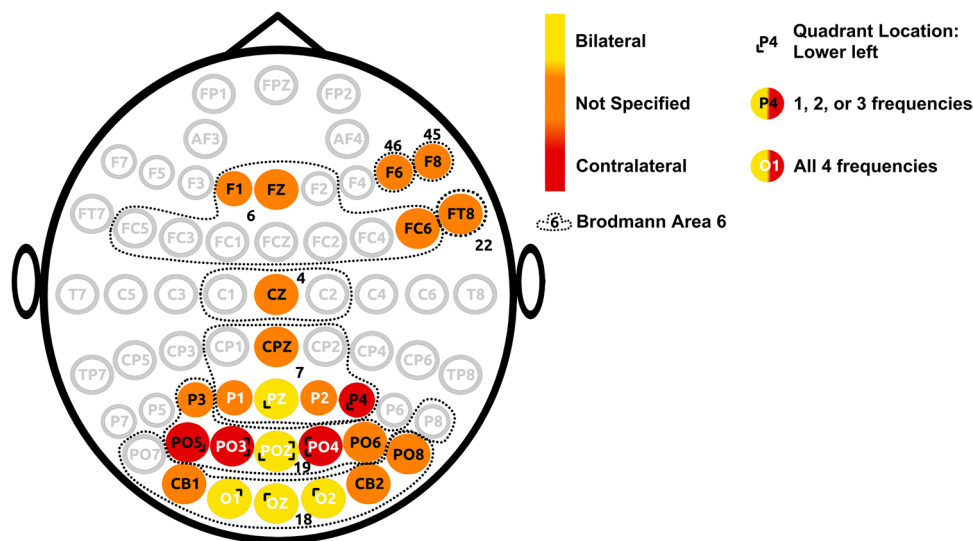
## Discussion

In this paper, we first reviewed the source localization of cortical generators induced by four widely used BCI paradigms. The closest EEG electrodes were then computed for each of these task-dependent neuronal sources. Our objective



**Table 5** 3D Talairach coordinates of the two significant cluster maxima for steady-state visual potentials depending on the visual stimulus location on the screen. The available data did not allow calculations of the Cohen's *d* effect size per electrode.

Quadrant location	Lobe	Macro-anatomical structure	Laterality	BA	Hem	Talairach			Closest electrode(s)
						X	Y	Z	
Upper left	Right occipital	Middle occipital gyrus	Bilateral	18	R	13	-92	-9	O2, OZ
		Superior occipital gyrus	Contralateral	19	R	36	-71	-4	PO4
Lower left	Median parieto-occipital	Superior parietal lobule, cuneus	Bilateral	7, 19	R	5	-74	2	PZ, POZ
	Right parieto-occipital	Inferior parietal lobule, superior occipital gyrus	Contralateral	7, 19	R	38	-65	0	P4, PO4
Upper right	Median occipital	Cuneus	Bilateral	19	L	-9	-86	-7	POZ, O1
	Left occipital	Superior occipital gyrus	Contralateral	19	L	-35	-73	-5	PO3
Lower right	Left Occipital	Cuneus	Bilateral	19	L	-6	-80	3	POZ
		Superior occipital gyrus	Contralateral	19	L	-31	-64	8	PO3, PO5

**Fig. 4** Steady-state visual evoked potential paradigm: Activated electrodes with their Brodmann areas and brain laterality linked to quadrant location or full-screen frequency

is to create a paradigm-based channel selection framework that could be used as a reference by any EEG researcher.

### Inter-subject variability

Brain atlases are becoming more ubiquitous in the field of neuroscience because they provide a reference framework for the analysis and visualization of neuroimaging data. By nature, the human cerebral cortex is deeply convoluted, and its folding pattern presents dramatic inter-subject variability (Van Essen & Dierker, 2007). Brain size and shape, as well as the dimension of cortical areas, also differ drastically across individuals (Andrews et al., 1997). Quantification of the inter-subject variability of functional connectivity has demonstrated a nonuniform distribution across brain regions.

The prefrontal and temporoparietal regions exhibit the highest level of variability, whereas the sensorimotor and visual networks show the lowest level (Mueller et al., 2013). The higher variability in the former regions is hypothesized to indicate the larger influence of environmental or epigenetic over purely genetic factors. Conversely, the latter regions seem to represent the hallmarks of common mammalian brain evolution and development (Zilles & Amunts, 2013).

The estimated EEG electrodes corresponding to known cortical generators do not hold identical significance probability. The lower inter-subject variability of sensorimotor and visual networks should be more constant across subjects and result in a higher average accuracy for BCI classification. Assuming the repeatability of the motor or visual task performed by the subject, the estimated EEG electrodes

**Table 6** 3D Talairach coordinates of significant cluster maxima for the P3b component of the P300 event-related potential; NP: not pertinent; BA: Brodmann area; Cohen's *d* mean effect size with a 95% confidence interval and the number of relevant studies in superscript

Time (in ms)	Contribution		Lobe	Anatomic areas	Area	Main macro-anatomical structures	BA	Talairach			Closest electrode(s)	Cohen's <i>d</i> weighted effect size
								X	Y	Z		
230–280	Low	Frontal	Prefrontal cortex	Inferior frontal Superior frontal	Inferior frontal gyrus Superior frontal gyrus Precentral gyrus Middle frontal gyrus		9 8, 9 44 6 6, 9	-64 -39 40 44 -24 32	19 42 43 17 -4 0	15 39 36 6 57 56	F5, FC5 F3, AF3 F4, AF4 F8 FC1, FC3 FC4	3.27 [1.67; 4.87] <sup>1</sup> 3.48 [1.65; 5.57] <sup>1</sup> 4.4 [2.48; 6.4] <sup>1</sup> 3.27 [1.67; 4.87] <sup>1</sup> NA 2.86 [1.26; 4.46] <sup>1</sup>
230–280	NA	430–480	Premotor and motor cortex	Dorso-lateral prefrontal cortex	Medial pre-motor SMA Cingulate cortex Primary motor (M1) Primary sensory (S1)		11 32, 6 6, 24 6 1, 2, 3	-3 -3 -1 24 62	38 10 3 -16 -34	-13 46 56 52 24	FZ, FPZ FCZ FCZ C2 C4	NA 3.45 [1.82; 5.47] <sup>2</sup> 3.45 [1.82; 5.47] <sup>2</sup> 2.44 [1.13; 3.75] <sup>1</sup> 3.5 [2.32; 4.68] <sup>1</sup> 3.13 [1.8; 4.46] <sup>2</sup> 3.3 [1.82; 4.95] <sup>3</sup> 4.78 [3.31; 6.44] <sup>3</sup> 4.28 [2.85; 5.97] <sup>3</sup> 3.98 [2.52; 5.51] <sup>4</sup>
230–280	High	Parietal	Inferior parietal lobule	Supramarginal gyrus		40	-47	-45	43	CP3	CP3	3.3 [1.82; 4.95] <sup>3</sup> 4.78 [3.31; 6.44] <sup>3</sup> 4.28 [2.85; 5.97] <sup>3</sup> 3.98 [2.52; 5.51] <sup>4</sup>
230–280	430–480	Posterior parietal cortex	Superior parietal lobule			7, 19	-30	-73	44	P1, P3	P1, P3	3.98 [2.52; 5.51] <sup>4</sup>

**Table 6** (continued)

Time (in ms)	Contribution	Lobe	Anatomic areas	Area	Main macro-anatomical structures	BA	Talairach			Closest electrode(s)	Cohen's <i>d</i> weighted effect size
							X	Y	Z		
230–280	High	Temporal		Inferior temporal	Fusiform gyrus	19, 37	-38	-60	-16	P7	4.97 [3.53; 6.83] <sup>2</sup>
230–280	NA			Middle temporal	Middle temporal gyrus	21	-59	-18	-13	T7, TP7	NA
230–280	NA			Superior temporal	Superior temporal sulcus	40, 39	52	-44	14	CP4, P6	4.87 [3.44; 6.56] <sup>3</sup>
230–280	NA				Cuneus	19	20	-82	36	PO4, O2	3.79 [2.07; 5.49] <sup>2</sup>
230–280	NA	Occipital		Inferior occipital	Lingual gyrus	19	-29	-76	-3	PO3, O1	4.31 [2.37; 6.23] <sup>2</sup>
230–280	NA	Subcortical regions	Thalamus	Median occipital		18	-1	-76	2	OZ	4.01 [2.09; 5.9] <sup>2</sup>
230–280	NA	Subcortical regions	Insula			13	-45	11	5	NP	NP

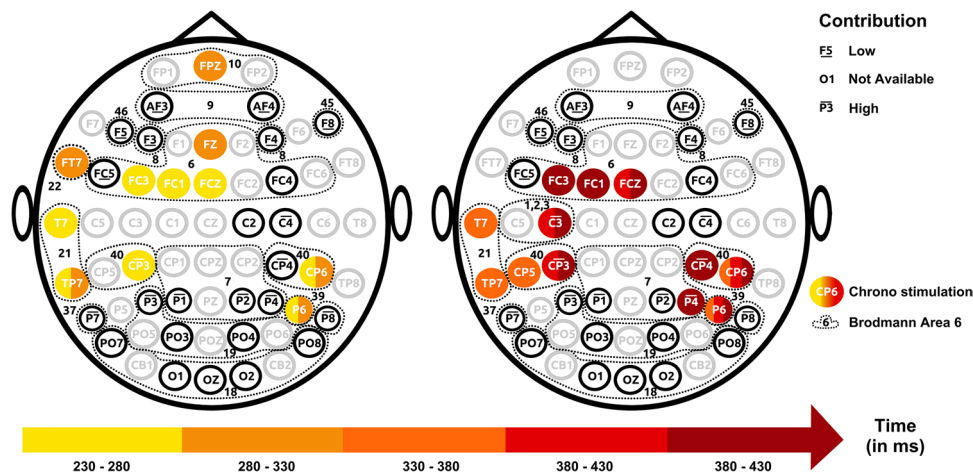


**Fig. 5** P3b component of the P300 paradigm: Electrodes' level and chronology of activation with corresponding Brodmann areas

for an individual can be hypothesized to remain mostly unchanged over time and across sessions if they belong to motor (BA 4, 6, 8), sensory (BA 1, 2, 3, 5, 40), or visual (BA 17, 18, 19) regions. For electrodes that are part of other brain areas, more variability should be expected between subjects.

### Equivalent current dipole

Scalp EEG electrodes are generally believed to record macroscopic postsynaptic potentials created by assemblies of pyramidal cells of the neocortex (mostly located in cortical layers III, V, and VI) (Olejniczak, 2006). To measure this generated electric field at a distance from the sources, the underlying neuronal currents must be well organized in space and time. The estimation of cortical generators corresponding to a certain distribution of electrical potentials recorded at the scalp is an ill-posed problem, known as the inverse problem. Different models of the neuronal sources and of the volume conductor have been investigated to estimate approximate solutions. Most neurophysiological findings are based on the simplest source model, namely the equivalent current dipole. Because of the columnar organization of the cortex, the resulting EEG potential is assumed to behave as if it were produced by normally oriented current dipoles over the entire cortical sheet (da Silva, 2004; Attal et al., 2009).

An equivalent dipole approximates the barycenter of the corresponding active cortical area at a given time with no appreciable delay in the scalp sensor measurement. Assuming that the signal propagates linearly and instantaneously inside a homogeneous and isotropic medium, both the position and orientation of the dipole affect the potential scalp spatial pattern. If the dipole is radial to the scalp surface or located in superficial cortical areas, the closest EEG electrode should record the highest potential activity regardless of its orientation. For a deeper tangential dipole, the

maximum amplitude would be recorded at a neighboring electrode (Congedo, 2013). Hence, under the linear conduction model assumption, the closest EEG electrode or its neighbors should receive most of the signal generated by the underlying cortical generator.

### Signal-to-noise ratio

Four main types of noise affect the recorded EEG signals. Instrumental noise might arise from equipment but is typically low and is considered to be uncorrelated with the signals. Environmental noise is routinely avoided by acquiring the data in a sound-attenuated and electromagnetically shielded EEG chamber. Biological noise emerging from extra-cerebral artifacts, such as blinks or muscle movements, may be removed using preprocessing algorithms, such as ICA (Shen et al., 2002) or ABC (Guttmann-Flury et al., 2019). We presume that the channel selection procedure is applied to cleaned data, free from these three types of noise. However, the underlying cerebral background noise is still present and accounts for most of the EEG signals.

Conventionally, background noise summarizes all spontaneous neural activity of various magnitudes and frequencies unrelated to the task at hand. With the hypothesis that this noise is generated from randomly distributed and statistically independent stationary dipole sources, averaging single events should yield the reproducible part of the signals and cancel the noise. Thus, time-locked averaging to a stimulus (visual or auditory) can be used to determine the locations and time courses of the relevant sources with a high signal-to-noise ratio (SNR) (de Munck et al., 2002). Latency adjusted averaging can also be used to enhance the SNR of evoked responses (e.g., by applying an adequate narrow-band Gaussian filter) (de Munck et al., 2002; Burghoff et al., 2005). Furthermore, SNR can be improved by channel selection,

which may also increase classification accuracy and reduce computational complexity. Assuming that close electrodes record similar background noise, subtracting a low-SNR neighboring electrode from a selected one might meliorate the SNR, and, thus, the accuracy (Wang et al., 2004).

## Limitations

This review summarizes the results from 21 studies. Each paradigm uses the same type of task; however, different conditions or experimental setups might alter the homogeneity of the results. For example, in the MI paradigm, subjects were asked to imagine flexion or extension of single fingers, specific finger movements, or precision grasping of objects.

Additionally, the participants' demographics are biased towards right-handedness; more specifically, in the visual-related experiments (SSVEP or P300), no article mentions left-handed participants. For motor-related experiments (MI or ME), specifying right-handedness as an inclusion criterion accounts for 62% of the reviewed papers but 24% do not report on it, 9% mention both, and 5% refer to left-handedness only. Nevertheless, the effects of handedness have been well established in the motor areas (Zapała et al., 2020) and, to a lesser degree, in the visual areas (Willems et al., 2010). Hence, the results derived from these studies should be applied carefully, and the linked variability must be considered.

For motor-related tasks, participants were instructed to use their dominant, nondominant, or both hands depending on the paradigm. These conditions yield a hand-dependent heterogeneity. Figure 6 illustrates this issue for four of the reviewed studies on electrode FC1 during an MI task. For this electrode, data were only available for right-handed subjects. The individuals' Cohen's  $d$  effect sizes were

clearly greater when using the dominant hand compared to the left hand. As a consequence, the right-weighted mean effect size differed from the left one. However, for most electrodes, data were insufficient to generalize the observations. To harmonize the results, the weighted mean effect size for both hands were only reported in Tables 2 and 3.

Moreover, the data acquisition was usually executed during a single session. Inter-session variability has been highlighted for time-varying brain functions (resting state networks) (Meyer et al., 2013). Considering the dynamic aspect of task learning involved in most BCI paradigms, the average cortical locations probably vary for a single subject across time and across sessions (Chervyakov et al., 2016). The procedure of averaging over trials is arguably suboptimal but is still the most commonly used. Intra-subject variability, as a result, is mostly unaccounted for in this review.

This variability issue is also reflected in the Cohen's  $d$  effect size. For one study (Ramirez-Quintana et al., 2020), the corresponding author provided the raw data from eight subjects who performed 34 trials each. Thus, it was possible to calculate the effect size by averaging all trials regardless of which subject performed the action ( $N=272$ ). To compare, the ERP was computed for each subject, and the resulting values were used to determine the effect size across subjects ( $N=8$ ). The obtained subject-dependent effect size ( $5.18 \pm 1.1$ ) proved to be much larger than the trial-dependent effect size ( $1.39 \pm 0.05$ ), in which the means were obtained from electrode O1 and displayed with their standard error. This highlights the greater intra-subject variability compared to the inter-subject one.

When averaging over all trials for a specific subject, the signal of interest stands out while the noise decreases. Theoretically, a high number of trials would completely cancel the noise. A researcher might favor a type of calculation

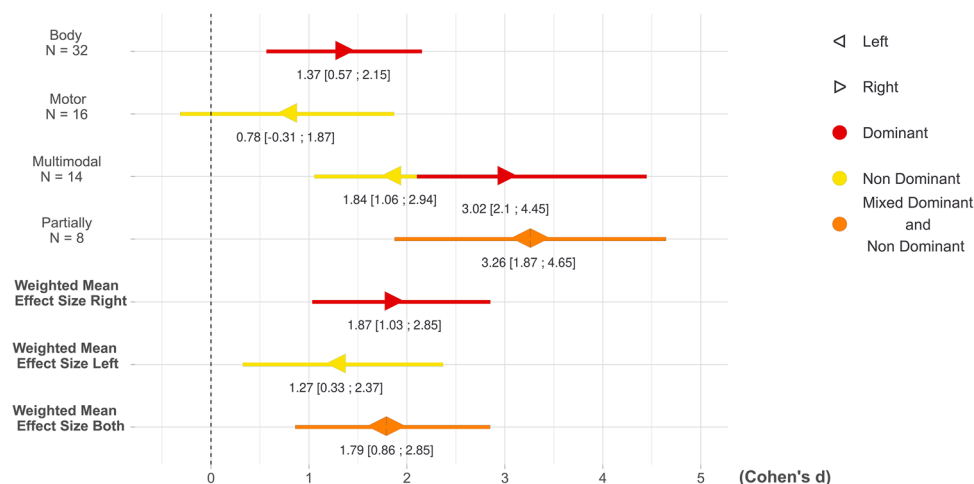


**Fig. 6** Cohen's  $d$  effect size per study for MI task on electrode FC1 and weighted mean effect size according to the subject handedness, hand used, and sample size  $N$  (number of subjects)

depending on the application the study is aimed at. To characterize an ERP, one might prefer to average per subject to remove intra-subject variability and to get a noise-free signal. When designing a new study, the weighted mean effect size could be used to predict the minimum number of subjects to include in the experiment. However, it should be noted that, because nearly all reviewed studies compute subject-dependent averages, the results shown in the tables are only valid for similar computations.

## Conclusion

The current review summarizes the subsets of EEG electrodes corresponding to the most significant cortical source activations. Sample sizes were estimated depending on the effect sizes values to obtain a statistical power of 80%. For every electrode, the weighted mean Cohen's  $d$  provides the magnitude of the corresponding effect size. It should be noted that each element in a subset must have a large Cohen's  $d$  with a high lower bound confidence interval, confirming its significance.

For each of the four commonly used BCI paradigms—MI, ME, SSVEP, and P300—the core channel selection (CCS) was extracted from the defined groups. These CCS allow implementing semiparametric algorithms that could adapt to various modalities of these paradigms. A meta-analysis with a greater number of studies would lead to more specifically adapted and extended subsets. Ideally, this meta-analysis should be followed by a sufficiently powered experiment that would assess the validity of the different CCS. It could also be interesting to compare the CCS to other data-driven channel selection methods.

A relevant definition of subsets would replace the non-parametric channel selection procedure while reducing the computational complexity and optimizing the BCI accuracy. This knowledge-based channel selection framework would have the advantages of practicality and rapidity, allowing for an easy implementation.

**Acknowledgements** This work is supported in part by the National Key R&D Program of China (Grant No. 2020YFC2007800), the National Natural Science Foundation of China (Grant No. 51905339, No. 51620105002), and the Science and Technology Commission of Shanghai Municipality (Grant No. 18JC1410400).

## Declarations

**Conflict of interest** No competing interests to declare.

## References

- Aine, C. J. (1995). A conceptual overview and critique of functional neuroimaging techniques in humans: I. MRI/fMRI and PET. *Critical Reviews in Neurobiology*, 9, 229–309.
- Alotaiby, T., El-Samie, F. E. A., Alshebeili, S. A., & Ahmad, I. (2015). A review of channel selection algorithms for EEG signal processing. *EURASIP Journal on Advances in Signal Processing*, 2015, 66.
- Andrews, T. J., Halpern, S. D., & Purves, D. (1997). Correlated size variations in human visual cortex, lateral geniculate nucleus, and optic tract. *The Journal of Neuroscience*, 17, 2859–2868.
- Ardekani, B. A., et al. (2002). Functional magnetic resonance imaging of brain activity in the visual oddball task. *Cognitive Brain Research*, 14, 347–356.
- Arns, M., Conners, C. K., & Kraemer, H. C. (2013). A Decade of EEG theta/beta ratio research in ADHD: A meta-analysis. *Journal of Attention Disorders*, 17, 374–383.
- Arvaneh, M., Guan, C., Ang, K. K., & Quek, C. (2010). Optimizing EEG channel selection by regularized spatial filtering and multi band signal decomposition. *Biomedical Engineering*, 7.
- Attal, Y., et al. (2009). Modelling and detecting deep brain activity with MEG and EEG. *IRBM*, 30, 133–138.
- Barachant, A., & Bonnet, S. (2011). Channel selection procedure using riemannian distance for BCI applications. In *2011 5th International IEEE/EMBS Conference on Neural Engineering* (pp. 348–351). <https://doi.org/10.1109/NER.2011.5910558>
- Begliomini, C., Nelini, C., Caria, A., Grodd, W., & Castiello, U. (2008). Cortical activations in humans grasp-related areas depend on hand used and handedness. *PLoS ONE*, 3.
- Begliomini, C., Sartori, L., Di Bono, M. G., Budisavljević, S., & Castiello, U. (2018). The neural correlates of grasping in left-handers: When handedness does not matter. *Frontiers in Neuroscience*, 12.
- Ben-Shachar, M. S., Lüdtke, D., & Makowski, D. (2020). effectsize: Estimation of effect size indices and standardized parameters. *Journal of Open Source Software*, 5, 2815.
- Bledowski, C., et al. (2004). Localizing P300 generators in visual target and distractor processing: A combined event-related potential and functional magnetic resonance imaging study. *The Journal of Neuroscience*, 24, 9353–9360.
- Blinowska, K., et al. (2009). Multimodal imaging of human brain activity: Rational, biophysical aspects and modes of integration. *Computational Intelligence and Neuroscience*, 2009, e813607 <https://www.hindawi.com/journals/cin/2009/813607/>
- Bos, D. P., et al. (2010). Human-computer interaction for BCI games: Usability and user experience. In *2010 International Conference on Cyberworlds* (pp. 277–281). <https://doi.org/10.1109/CW.2010.22>
- Burghoff, M., et al. (2005). A template-free approach for determining the latency of single events of auditory evoked M100. *Physics in Medicine and Biology*, 50, N43–N48.
- Burianová, H., et al. (2013). Multimodal functional imaging of motor imagery using a novel paradigm. *NeuroImage*, 71, 50–58.
- Cabeza, R., & Nyberg, L. (2000). Imaging Cognition II: An Empirical Review of 275 PET and fMRI Studies. *Journal of Cognitive Neuroscience*, 12, 1–47.
- Chaudhary, U., Birbaumer, N., & Ramos-Murguialday, A. (2016). Brain-computer interfaces for communication and rehabilitation. *Nature Reviews. Neurology*, 12, 513–525.
- Chervyakov, A. V., Sinitsyn, D. O., & Piradov, M. A. (2016). Variability of neuronal responses: Types and functional significance in neuroplasticity and neural darwinism. *Frontiers in Human Neuroscience*, 10.



- Clark, V. P., Fannon, S., Lai, S., Benson, R., & Bauer, L. (2000). Responses to rare visual target and distractor stimuli using event-related fMRI. *Journal of Neurophysiology*, 83, 3133–3139.
- Cohen, J. (1977). *Statistical power analysis for the behavioral sciences*. Elsevier. <https://doi.org/10.1016/C2013-0-10517-X>
- Congedo, M. (2013). *EEG source analysis*. Université de Grenoble.
- Crammond, D. J. (1997). Motor imagery: never in your wildest dream. *Trends in Neurosciences*, 20, 54–57.
- Curran, E. A., & Stokes, M. J. (2003). Learning to control brain activity: A review of the production and control of EEG components for driving brain–computer interface (BCI) systems. *Brain and Cognition*, 51, 326–336.
- da Silva, L. (2004). F. Functional localization of brain sources using EEG and/or MEG data: volume conductor and source models. *Magnetic Resonance Imaging*, 22(1533–1538).
- da Silva, L. (2013). F. EEG and MEG: Relevance to neuroscience. *Neuron*, 80, 1112–1128.
- Danckert, J., et al. (2002). Selective, non-lateralized impairment of motor imagery following right parietal damage. *Neurocase*, 8, 194–204.
- de Munck, J. C., Huizenga, H. M., Waldorp, L. J., & Heethaar, R. A. (2002). Estimating stationary dipoles from MEG/EEG data contaminated with spatially and temporally correlated background noise. *IEEE Transactions on Signal Processing*, 50, 1565–1572.
- Dresel, C., et al. (2005). The functional neuroanatomy of coordinated orofacial movements: Sparse sampling fMRI of whistling. *NeuroImage*, 28, 588–597.
- Eccleston, C., Williams, A. C. de C., & Morley, S. (2009). Psychological therapies for the management of chronic pain (excluding headache) in adults. *Cochrane Database of Systematic Reviews*. <https://doi.org/10.1002/14651858.CD007407.pub2>
- Ellis, P. D. (2010). *The essential guide to effect sizes: Statistical power, meta-analysis, and the interpretation of research results*. (Cambridge University Press. <https://doi.org/10.1017/CBO9780511761676>
- Fjell, A. M., & Walhovd, K. B. (2004). Life-span changes in P3a. *Psychophysiology*, 41, 575–583.
- Friedman, D. (2003). Cognition and aging: A highly selective overview of event-related potential (ERP) Data. *Journal of Clinical and Experimental Neuropsychology*, 25, 702–720.
- Gaeta, H., Friedman, D., & Hunt, G. (2003). Stimulus characteristics and task category dissociate the anterior and posterior aspects of the novelty P3. *Psychophysiology*, 40, 198–208.
- Gerardin, E., et al. (2000). Partially overlapping neural networks for real and imagined hand movements. *Cerebral Cortex*, 10, 1093–1104.
- Ghaemi, A., Rashedi, E., Pourrahimi, A. M., Kamandar, M., & Rahdari, F. (2017). Automatic channel selection in EEG signals for classification of left or right hand movement in Brain Computer Interfaces using improved binary gravitation search algorithm. *Biomedical Signal Processing and Control*, 33, 109–118.
- González-Mendoza, A., Pérez-Benítez, J. L., Pérez-Benítez, J. A., & Espina-Hernández, J. H. (2015). Brain computer interface based on SSVEP for controlling a remote control car. In *2015 International Conference on Electronics, Communications and Computers (CONIELECOMP)* (pp. 93–97). <https://doi.org/10.1109/CONIELECOMP.2015.7086931>
- Grafton, S. T., Arbib, M. A., Fadiga, L., & Rizzolatti, G. (1996). Localization of grasp representations in humans by positron emission tomography. *Experimental Brain Research*, 112, 103–111.
- Curve, D., et al. (2020). Subject-specific EEG channel selection using non-negative matrix factorization for lower-limb motor imagery recognition. *Journal of Neural Engineering*, 17, 026029.
- Guttmann-Flury, E., Sheng, X., Zhang, D., & Zhu, X. (2019). A new algorithm for blink correction adaptive to inter- and intra-subject variability. *Computers in Biology and Medicine*, 114, 103442.
- Halder, S., et al. (2011). Neural mechanisms of brain–computer interface control. *NeuroImage*, 55, 1779–1790.
- Hardwick, R. M., Caspers, S., Eickhoff, S. B., & Swinnen, S. P. (2017). Neural correlates of motor imagery, action observation, and movement execution: A comparison across quantitative meta-analyses. *bioRxiv*, 198432. <https://doi.org/10.1101/198432>
- He, L., Yu, Z., Gu, Z., & Li, Y. (2009). *Bhattacharyya bound based channel selection for classification of motor imageries in EEG signals*. <https://doi.org/10.1109/CCDC.2009.5192711>
- Hedges, L. V., & Pigott, T. D. (2001). The power of statistical tests in meta-analysis. *Psychological Methods*, 6, 203–217.
- Hill, N. J., & Wolpaw, J. R. (2016). Brain–computer interface☆. In *Reference module in biomedical sciences*. Elsevier. <https://doi.org/10.1016/B978-0-12-801238-3.99322-X>
- Hunter, J. E., & Schmidt, F. L. (2000). Fixed effects vs. random effects meta-analysis models: Implications for cumulative research knowledge. *International Journal of Selection and Assessment*, 8, 275–292.
- Ikegami, S. M., Takano, K., Wada, M. M., Saeki, N. M., & Kansaku, K. (2012). Effect of the green/blue flicker matrix for P300-based brain–computer interface: An EEG–fMRI study. *Frontiers in Neurology*, 3.
- Jurcak, V., Tsuzuki, D., & Dan, I. (2007). 10/20, 10/10, and 10/5 systems revisited: Their validity as relative head-surface-based positioning systems. *NeuroImage*, 34, 1600–1611.
- Kaplan, A. Y., Shishkin, S. L., Ganin, I. P., Basyul, I. A., & Zhigalov, A. Y. (2013). Adapting the P300-based brain–computer interface for gaming: A review. *IEEE Transactions on Computational Intelligence in AI and Games*, 5, 141–149.
- Koessler, L., et al. (2009). Automated cortical projection of EEG sensors: Anatomical correlation via the international 10–10 system. *NeuroImage*, 46, 64–72.
- Kraeutner, S., Gionfriddo, A., Bardouille, T., & Boe, S. (2014). Motor imagery-based brain activity parallels that of motor execution: Evidence from magnetic source imaging of cortical oscillations. *Brain Research*, 1588, 81–91.
- Krolak-Salmon, P., et al. (2003). Human lateral geniculate nucleus and visual cortex respond to screen flicker. *Annals of Neurology*, 53, 73–80.
- Króliczak, G., Piper, B. J., & Frey, S. H. (2016). Specialization of the left supramarginal gyrus for hand-independent praxis representation is not related to hand dominance. *Neuropsychologia*, 93, 501–512.
- Lal, T. N., et al. (2004). Support vector channel selection in BCI. *IEEE Transactions on Biomedical Engineering*, 51, 1003–1010.
- Leeb, R., et al. (2006). Walking by thinking: The brainwaves are crucial, not the muscles! *Presence Teleoperators and Virtual Environments*, 15, 500–514.
- Li, M., Ma, J., & Jia, S. (2011). Optimal combination of channels selection based on common spatial pattern algorithm. In *2011 IEEE International Conference on Mechatronics and Automation* (pp. 295–300). <https://doi.org/10.1109/ICMA.2011.5985673>
- Liberati, A., et al. (2009). The PRISMA Statement for Reporting Systematic Reviews and Meta-Analyses of Studies That Evaluate Health Care Interventions: Explanation and Elaboration. *PLoS Medicine*, 6, e1000100.
- Luu, P., & Ferree, T. (2005). *Determination of the HydroCel geodesic sensor nets' average electrode positions and their 10 – 10 international equivalents*. Tech. note (p. 11). Electrical Geodesics, Inc.
- Martinez, P., Bakardjian, H., & Cichocki, A. (2007). Fully online multicommand brain–computer interface with visual neurofeedback using SSVEP paradigm. *Computational Intelligence and Neuroscience*, 2007, e94561 <https://www.hindawi.com/journals/cin/2007/094561/>



- Menon, V., Ford, J. M., Lim, K. O., Glover, G. H., & Pfefferbaum, A. (1997). Combined event-related fMRI and EEG evidence for temporal—parietal cortex activation during target detection. *NeuroReport*, 8, 3029–3037.
- Meyer, M. C., van Oort, E. S. B., & Barth, M. (2013). Electrophysiological correlation patterns of resting state networks in single subjects: A combined EEG–fMRI study. *Brain Topography*, 26, 98–109.
- Michel, C. M. (2004). EEG source imaging. *Clinical Neurophysiology*, 115, 2195–2222.
- Mokienko, O. A., et al. (2013). Increased motor cortex excitability during motor imagery in brain-computer interface trained subjects. *Frontiers in Computational Neuroscience*, 7.
- Mueller, S., et al. (2013). Individual variability in functional connectivity architecture of the human brain. *Neuron*, 77, 586–595.
- Mulert, C., et al. (2004). The neural basis of the P300 potential. *European Archives of Psychiatry and Clinical Neuroscience*, 254, 190–198.
- Müller, T., Ball, T., Kristeva-Feige, R., Mergner, T., & Timmer, J. (2000). Selecting relevant electrode positions for classification tasks based on the electro-encephalogram. *Medical & Biological Engineering & Computing*, 38, 62–67.
- Mullin, J. P., et al. (2016). Is SEEG safe? A systematic review and meta-analysis of stereo-electroencephalography-related complications. *Epilepsia*, 57, 386–401.
- Nicolas-Alonso, L. F., & Gomez-Gil, J. (2012). Brain computer interfaces, a review. *Sensors*, 12, 1211–1279.
- Nijboer, F., et al. (2008). An auditory brain–computer interface (BCI). *Journal of Neuroscience Methods*, 167, 43–50.
- Nunez, P. L., & Nunez, E. P. of B. E. P. L., Srinivasan, R., & Srinivasan, A. P. of C. S. R. (2006). *Electric fields of the brain: The neurophysics of EEG*. Oxford University Press.
- Olejniczak, P. (2006). Neurophysiologic basis of EEG. *Journal of Clinical Neurophysiology*, 23, 186–189.
- Oxley, T. J., et al. (2020). Motor neuroprosthesis implanted with neurointerventional surgery improves capacity for activities of daily living tasks in severe paralysis: first in-human experience. *Journal of NeuroInterventional Surgery*. <https://doi.org/10.1136/neurintsurg-2020-016862>
- Perlstein, W. M., et al. (2003). Steady-state visual evoked potentials reveal frontally-mediated working memory activity in humans. *Neuroscience Letters*, 342, 191–195.
- Pfurtscheller, G., & Neuper, C. (2001). Motor imagery and direct brain-computer communication. *Proceedings of the IEEE*, 89, 1123–1134.
- Poldrack, R. A., et al. (2017). Scanning the horizon: towards transparent and reproducible neuroimaging research. *Nature Reviews. Neuroscience*, 18, 115–126.
- Porro, C. A., Cettolo, V., Francescato, M. P., & Baraldi, P. (2000). Ipsilateral involvement of primary motor cortex during motor imagery. *The European Journal of Neuroscience*, 12, 3059–3063.
- Qi, F., et al. (2021). Spatiotemporal-filtering-based channel selection for single-trial EEG classification. *IEEE Transactions on Cybernetics*, 51, 558–567.
- Ramirez-Quintana, J. A., Madrid-Herrera, L., Chacon-Murguia, M. I., & Corral-Martinez, L. F. (2020). Brain-computer interface system based on P300 processing with convolutional neural network, novel speller, and low number of electrodes. *Cognitive Computation*. <https://doi.org/10.1007/s12559-020-09744-2>
- Regan, D. (1989). *Human brain electrophysiology: Evoked potentials and evoked magnetic fields in science and medicine*. Elsevier.
- Rizzolatti, G., & Craighero, L. (2004). The mirror-neuron system. *Annual Review of Neuroscience*, 27, 169–192.
- Rossini, P. M., Rossi, S., Babiloni, C., & Polich, J. (2007). Clinical neurophysiology of aging brain: From normal aging to neurodegeneration. *Progress in Neurobiology*, 83, 375–400.
- Russo, F. D., et al. (2007). Spatiotemporal analysis of the cortical sources of the steady-state visual evoked potential. *Human Brain Mapping*, 28, 323–334.
- Sacchet, M. D., & Knutson, B. (2013). Spatial smoothing systematically biases the localization of reward-related brain activity. *NeuroImage*, 270–277.
- Schalk, G., & Leuthardt, E. C. (2011). Brain-computer interfaces using electrocorticographic signals. *IEEE Reviews in Biomedical Engineering*, 4, 140–154.
- Schippers, M. B., & Keysers, C. (2011). Mapping the flow of information within the putative mirror neuron system during gesture observation. *NeuroImage*, 57, 37–44.
- Schmolsky, M. T., et al. (1998). Signal timing across the macaque visual system. *Journal of Neurophysiology*, 79, 3272–3278.
- Schröder, M., et al. (2005). Robust EEG channel selection across subjects for brain-computer interfaces. *EURASIP Journal on Advances in Signal Processing*, 2005, 3103–3112.
- Shen, M., Zhang, X., & Li, X. (2002). Independent component analysis of electroencephalographic signals. In *6th International Conference on Signal Processing*, 2002 (Vol. 2, pp. 1548–1551).
- Sitaram, R., et al. (2007). fMRI brain-computer interface: A tool for neuroscientific research and treatment. *Computational Intelligence and Neuroscience*, 2007, e25487 <https://www.hindawi.com/journals/cin/2007/025487/>
- Snyder, S. M., & Hall, J. R. (2006). A meta-analysis of quantitative EEG power associated with attention-deficit hyperactivity disorder. *Journal of Clinical Neurophysiology*, 23, 441–456.
- Spataro, R., et al. (2017). Reaching and grasping a glass of water by locked-in ALS patients through a BCI-controlled humanoid robot. *Frontiers in Human Neuroscience*, 11.
- Spencer, K. M., Dien, J., & Donchin, E. (2001). Spatiotemporal analysis of the late ERP responses to deviant stimuli. *Psychophysiology*, 38, 343–358.
- Srinivasan, R., Bibi, F. A., & Nunez, P. L. (2006). Steady-state visual evoked potentials: Distributed local sources and wave-like dynamics are sensitive to flicker frequency. *Brain Topography*, 18, 167–187.
- Srinivasan, R., Fornari, E., Knyazeva, M. G., Meuli, R., & Maeder, P. (2007). fMRI responses in medial frontal cortex that depend on the temporal frequency of visual input. *Experimental Brain Research*, 180, 677–691.
- Stippich, C., Ochmann, H., & Sartor, K. (2002). Somatotopic mapping of the human primary sensorimotor cortex during motor imagery and motor execution by functional magnetic resonance imaging. *Neuroscience Letters*, 331, 50–54.
- Torres, E. P., Torres, E. A., Hernández-Álvarez, M., & Yoo, S. G. (2020). EEG-based BCI emotion recognition: A survey. *Sensors*, 20, 5083.
- Tsui, C. S. L., Gan, J. Q., & Hu, H. (2011). A self-paced motor imagery based brain-computer interface for robotic wheelchair control. *Clinical EEG and Neuroscience*, 42, 225–229.
- Valentine, J. C., Pigott, T. D., & Rothstein, H. R. (2010). How many studies do you need?: A primer on statistical power for meta-analysis. *Journal of Educational and Behavioral Statistics*, 35, 215–247.
- Vallabhaneni, A., Wang, T., & He, B. (2005). Brain—computer interface. In B. He (Ed.), *Neural engineering* (pp. 85–121). Springer US. [https://doi.org/10.1007/0-306-48610-5\\_3](https://doi.org/10.1007/0-306-48610-5_3)
- van Erp, J., Lotte, F., & Tangermann, M. (2012). Brain-computer interfaces: Beyond medical applications. *Computer*, 45, 26–34.
- Van Essen, D. C., & Dierker, D. L. (2007). Surface-based and probabilistic atlases of primate cerebral cortex. *Neuron*, 56, 209–225.
- Vargas, C. D., et al. (2004). The influence of hand posture on corticospinal excitability during motor imagery: A transcranial magnetic stimulation study. *Cerebral Cortex*, 14, 1200–1206.

- Varney, N. R., & Damasio, H. (1987). Locus of Lesion in impaired pantomime recognition. *Cortex*, 23, 699–703.
- von Büna, P., Meinecke, F. C., Scholler, S., & Müller, K. (2010). Finding stationary brain sources in EEG data. In *2010 Annual International Conference of the IEEE Engineering in Medicine and Biology* (pp. 2810–2813). <https://doi.org/10.1109/IEMBS.2010.5626537>
- Waldert, S., et al. (2009). A review on directional information in neural signals for brain-machine interfaces. *Journal of Physiology, Paris*, 103, 244–254.
- Wang, Y., Zhang, Z., Gao, X., & Gao, S. (2004). Lead selection for SSVEP-based brain-computer interface. In *The 26th Annual International Conference of the IEEE Engineering in Medicine and Biology Society* (Vol. 2, pp. 4507–4510).
- Wang, L., Zhang, X., Zhong, X., & Zhang, Y. (2013). Analysis and classification of speech imagery EEG for BCI. *Biomedical Signal Processing and Control*, 8, 901–908.
- Ward, N. S., & Frackowiak, R. S. J. (2003). Age-related changes in the neural correlates of motor performance. *Brain*, 126, 873–888.
- West, R., Schwarb, H., & Johnson, B. N. (2010). The influence of age and individual differences in executive function on stimulus processing in the oddball task. *Cortex*, 46, 550–563.
- Willems, R. M., Toni, I., Hagoort, P., & Casasanto, D. (2009). Body-specific motor imagery of hand actions: neural evidence from right- and left-handers. *Frontiers in Human Neuroscience*, 3.
- Willems, R. M., Peelen, M. V., & Hagoort, P. (2010). Cerebral lateralization of face-selective and body-selective visual areas depends on handedness. *Cerebral Cortex*, 20, 1719–1725.
- Wolpaw, J. R., Birbaumer, N., McFarland, D. J., Pfurtscheller, G., & Vaughan, T. M. (2002). Brain-computer interfaces for communication and control. *Clinical Neurophysiology*, 113, 767–791.
- Zapała, D., et al. (2020). The effects of handedness on sensorimotor rhythm desynchronization and motor-imagery BCI control. *Scientific Reports*, 10, 2087.
- Zhu, D., Bieger, J., Garcia Molina, G., & Aarts, R. M. (2010). A survey of stimulation methods used in SSVEP-based BCIs. *Computational Intelligence and Neuroscience*, 2010, e702357 <https://www.hindawi.com/journals/cin/2010/702357/>
- Zilles, K., & Amunts, K. (2013). Individual variability is not noise. *Trends in Cognitive Sciences*, 17, 153–155.

**Open practices statement** The R code used to calculate the effect sizes per study and the weighted mean effect size is available online at <https://github.com/QinXinlan/review-effect-size>.

**Publisher's note** Springer Nature remains neutral with regard to jurisdictional claims in published maps and institutional affiliations.